Journal of Power Sources 195 (2010) 1747–1752

Contents lists available at ScienceDirect

Journal of Power Sources

journal homepage: www.elsevier.com/locate/jpowsour

Short communication

The preparation and performance of calcium carbide-derived carbon/polyaniline composite electrode material for supercapacitors

Liping Zheng[a], Ying Wang[b], Xianyou Wang[a,*], Na Li[a], Hongfang An[a], Huajie Chen[a], Jia Guo[b]

[a] School of Chemistry, Key Laboratory of Environmentally Friendly Chemistry and Applications of Minister of Education, Xiangtan University, Hunan 411105, China
[b] School of Chemical Engineering and Pharmacy, Wuhan Institute of Technology, Hubei 430073, China

ARTICLE INFO

Article history:
Received 25 July 2009
Received in revised form 7 September 2009
Accepted 30 September 2009
Available online 7 October 2009

Keywords:
Calcium carbide-derived carbon
Polyaniline
Composite electrode
Electrochemical performance
Supercapacitor

ABSTRACT

Calcium carbide (CaC_2)-derived carbon (CCDC)/polyaniline (PANI) composite materials are prepared by in situ chemical oxidation polymerization of an aniline solution containing well-dispersed CCDC. The structure and morphology of CCDC/PANI composite are characterized by Fourier infrared spectroscopy (FTIR), scanning electron microscope (SEM), transmission electron microscopy (TEM) and N_2 sorption isotherms. It has been found that PANI was uniformly deposited on the surface and the inner pores of CCDC. The supercapacitive behaviors of the CCDC/PANI composite materials are investigated with cyclic voltammetry (CV), galvanostatic charge/discharge and cycle life measurements. The results show that the CCDC/PANI composite electrodes have higher specific capacitances than the as grown CCDC electrodes and higher stability than the conducting polymers. The capacitance of CCDC/PANI composite electrode is as high as 713.4 F g^{-1} measured by cyclic voltammetry at 1 mV s^{-1}. Besides, the capacitance retention of coin supercapacitor remained 80.1% after 1000 cycles.

1. Introduction

Supercapacitors combining the advantages of the high power of dielectric capacitors and the high specific energy of rechargeable batteries have played an increasingly important role in power source applications such as hybrid electric vehicles and short-term power sources for mobile electronic devices [1]. According to energy storage mechanism, there are two types of supercapacitors, viz., electrochemical double layer capacitors (EDLCs) and redox supercapacitors. EDLCs have emerged as a promising energy storage option for applications that need high power along with exceptional storage and cycle life [2]. In the EDLCs, energy storage arises mainly from the accumulation of electronic and ionic charges at the interface between the electrode materials and the electrolyte solution. Therefore, the large surface area and the porosity of electrode active materials are the basic requirements to achieve high specific capacitance. Carbon materials have been considered as a good candidate for supercapacitors because of its high specific area, long cycle life, low cost and wide use in aqueous and nonaqueous solvents [3].

During the recent years, various carbonaceous materials have been widely used as electrode materials for EDLCs, such as activated organic materials [4], carbonized polymers [5], carbon aerogels [6], carbon fibers [7] and nanotubes [8]. All of the materials have different pore structures and surface chemistries due to the different processing techniques and starting materials. Recently, a new group of porous carbon materials, carbide-derived carbons (CDCs), in which non-carbon elements are selectively etched from the carbide via reaction with chlorine at elevated temperature, have been receiving attention in the literature for applications in EDLCs [9–11]. The CDCs have high specific surface area (SSA), with pore sizes that can be fine-tuned by controlling the chlorination temperature and by the choice of starting carbide. We have previously reported that the CaC_2-derived carbon (CCDC) with network structure was prepared by one-step route and used as electrode active material for supercapacitor [12].

Usually, the carbon materials only possess double layer capacitance, while metal oxide or conducting polymer possess Faradaic capacitance, and the Faradaic pseudocapacitance is almost 10–100 times higher than double layer capacitance [13]. Conducting polymers have been extensively studied as promising materials for electrochemical capacitors due to their redox chemistry and high conductivity in the doped state. In conducting polymers, electric energy can be stored and delivered as delocalized π-electrons are accepted and released during electrochemical doping/undoping, respectively. There are two types of doping process below [2]:

$$\text{p-doping}: (\text{polymer}) + yA^- \rightarrow [(\text{polymer})y^+yA^-] + ye^- \quad (1)$$

$$\text{n-doping}: (\text{polymer}) + yC^+ + ye^- \rightarrow [(\text{polymer})y^-yC^+] \quad (2)$$

* Corresponding author. Tel.: +86 731 58293043; fax: +86 731 58292282.
E-mail address: wxianyou@yahoo.com (X. Wang).

0378-7753/$ – see front matter © 2009 Elsevier B.V. All rights reserved.
doi:10.1016/j.jpowsour.2009.09.057

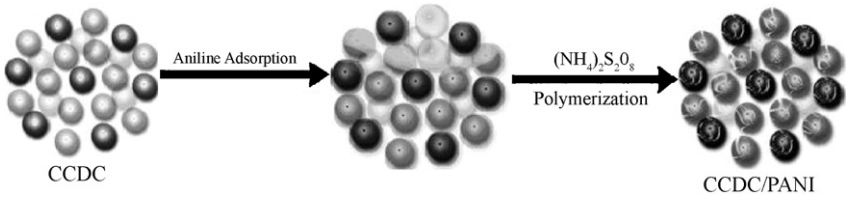

Fig. 1. Schematic preparing process of PANI on the surface of CCDC.

An improvement in the capacitance of carbon materials can be realized by preparing carbon-conducting polymer composites. Such a modification induces Faradaic pseudocapacitance effects apart from electrostatically charges accumulation. PANI has been used as the electrode materials of supercapacitors due to its oxidation–reduction properties, high SSA, environmental stability [14,15] as well as relatively easy polymerization in aqueous media.

Some researchers have demonstrated the suitability of PANI modification to improve the carbon materials capacitance and consequently, their applicability as electrodes in supercapacitors [15–18]. It is reported that the specific capacitances of the electrode active material for supercapacitors using PANI deposited on porous carbon is as high as 180 F g^{-1}, in comparison with a value of 92 F g^{-1} for the bare-carbon electrode [1]. Recently, our group prepared the polyaniline (PANI)/carbon aerogel (CA) composite electrode materials by chemical oxidation polymerization and obtained a high specific capacitance of 710.7 F g^{-1} [19].

Although some related works have been carried out on composites of activated carbon, CNTs and carbon fiber coated with PANI, there is less reported on fabricating CCDC/PANI composite by in situ chemical oxidative polymerization of an aniline solution containing well-dispersed CCDC and further characterizing on the supercapacitive behavior of the composites. The present study focuses on surface modification of CCDC with PANI by in situ chemical oxidation polymerization, as well as to determine the supercapacitive behaviors of the CCDC/PANI composite materials.

2. Experimental

2.1. Material synthesis

2.1.1. Synthesis of CCDC

The experimental setup used for synthesis of CaC_2-CDC (CCDC) has been reported in our previous work [12]. The precursor CaC_2 (formula weight 64.10 g mol^{-1}, density 2.22 g cm^{-3}) was obtained from Alfa Aesar. CaC_2 powder was placed in a quartz tube furnace. The tube was Ar purged for 30 min, then heated to the 400 °C at the heating rate of 6 °C min^{-1}, chlorine gas (freshly prepared gas in the laboratory) was directly passed through the tube furnace for 2 h. After chlorination, the furnace was cooled down to room temperature under an Ar purge at the condition of natural cooling.

2.1.2. Preparation of CCDC/PANI composites

The polyaniline coated CCDC was prepared by adsorption of aniline followed by in situ chemical polymerization with ammonium peroxodisulfate, its synthesis route of CCDC/PANI composite is schematically represented in Fig. 1. The detailed preparation process can be described as follows: (1) CCDC (0.5 g) was immersed in ethanol solution (100 mL, 20%, containing 1.4 g aniline and 10 g H_2SO_4) while being stirred under vacuum for 1 h; (2) ethanol solution (100 mL, 20%) was added to the above mentioned solution quickly with intensive stirring; (3) ammonium persulfate solution (the mass ratio of aniline/ammonium persulfate is 1:2.3) was added drop by drop to the solution mentioned in step 2 which was stirred at 0 °C for 5 h. The black-green product of the reaction was filtered and washed repeatedly with distilled water and alcohol. The resulting polymer was dried under vacuum at 50 °C for 24 h. The 70 wt.% of mass load of PANI in the composite was evaluated by calculating the weight difference of mesoporous carbon.

2.2. Measurement techniques for structural characterization

(1) The FTIR measurements of different samples were performed with a Fourier transform infrared (FTIR) spectrometer (Perkin-Elmer Spectrum one) in the wave number range from 4000 to 500 cm^{-1}, using the KBr disk method.
(2) The morphology of the CCDC/PANI composite was observed using a scanning electron microscope (JSE-6360LV).
(3) The transmission electron microscopy (TEM) of the CCDC/PANI composite was performed using a FEI Tecnai G2 microscope at 200 kV.
(4) Sorption analysis of porous carbon was done using N_2 as adsorbate at −196 °C with Quantachrome NovaWin2.

2.3. Preparation of the CCDC/PANI composite electrodes

The mixture containing 80 wt.% CCDC/PANI composite, 10 wt.% carbon black, and 10 wt.% polytetrafluoroethylene (PTFE) was well mixed, and then pressed onto a stainless-steel grid (1.6×10^7 Pa) that served as a current collector (area was 1.5 cm^2). The mass load of the as-prepared electrode was 5 mg cm^{-2}. The electrochemical performances of the electrodes were characterized by cyclic voltammetry (CV) and galvanostatic charge/discharge test. The used electrolyte was 1 M H_2SO_4 solution. The experiments were carried out using a three-electrode system, in which steel and the saturated calomel electrode (SCE, 0.242 V vs. the normal hydrogen electrode (NHE)) are used as counter and reference electrodes, respectively.

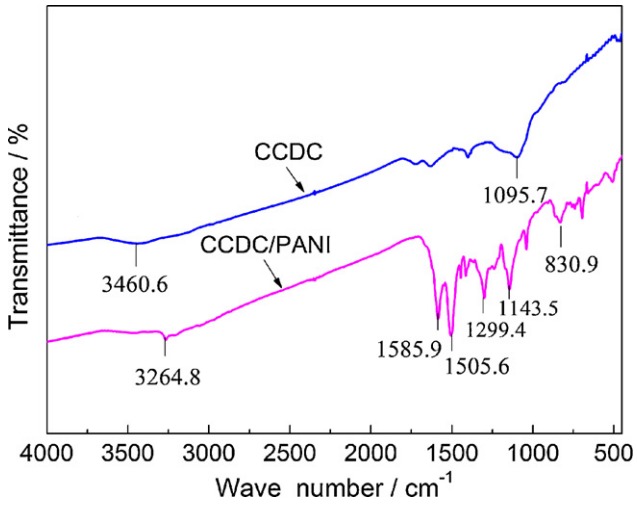

Fig. 2. FTIR spectra of CCDC and CCDC/PANI composite.

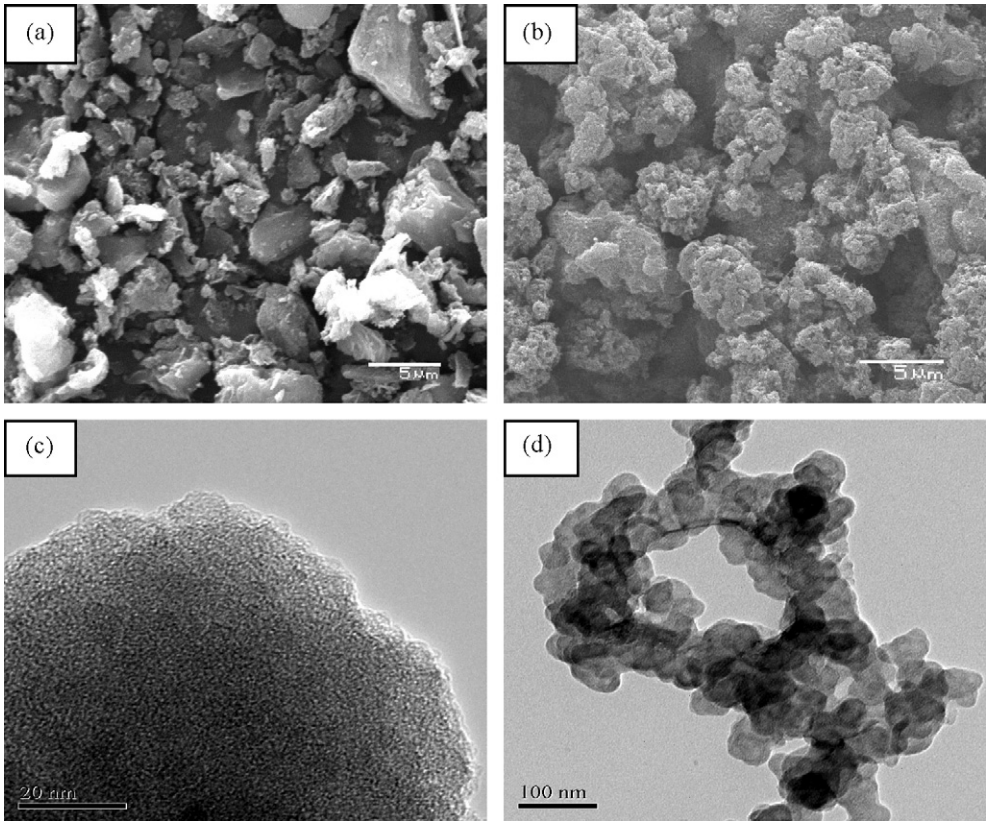

Fig. 3. SEM and TEM images of CCDC and CCDC/PANI composites. (a) SEM image of CCDC, (b) SEM image of CCDC/PANI, (c) TEM image of CCDC, (d) TEM image of CCDC/PANI.

3. Results and discussion

3.1. Material characterization

FTIR spectra of CCDC and CCDC/PANI composite are shown in Fig. 2. Characteristic peaks at 3460 and 1096 cm^{-1} are observed in the FTIR spectrum of the initial CCDC material. These peaks can be ascribed to –OH (3500 cm^{-1}) and C–C–O (1096 cm^{-1}) stretching vibration band, respectively. As to CCDC/PANI composite, the 1586 cm^{-1} band was characteristics of the nitrogen quinone (Q) structure, and 1506 cm^{-1} was related to the benzenoid structure (B). The bands in the range 1200–1400 cm^{-1} are the C–N stretching band of an aromatic amine, such as 1380 cm^{-1} (QBQ), 1340 cm^{-1} (QBQ, QBB, BBQ), and 1230 cm^{-1} (BBB) [20]. A strong band characteristically appears at 1144 cm^{-1}, which has been explained as an electronic band or vibration band of nitrogen quinone (N=Q=N). The C–H out of plane bending mode has been used as a key to identify the type of substituted benzene. This mode was observed in PANI as a single band at 831 cm^{-1}. This meant that PANI was 1,4 substituted. Comparing IR spectra in Fig. 2, it can be found that PANI exists apparently on the surface and micropore of CCDC.

The morphologies and microstructures of the CCDC and CCDC/PANI composite have been examined by scanning electron microscopy (SEM) and transmission electron microscopy (TEM). Fig. 3 shows SEM and TEM images of CCDC and CCDC/PANI composite. As being seen from Fig. 3(a), the as-prepared CCDC consisted of agglomerated small framework; while for the CCDC coated PANI (Fig. 3(b)), a layer of flocculent deposit coated homogenously the surface of CCDC, which was attributed to the freshly deposited PANI. The TEM image of the CCDC (Fig. 3(c)) is completely amorphous carbon with no detectable graphite layers, and has small particle size less than 5 nm and no agglomerated morphology. As shown in Fig. 3(d), it can be seen that a clear morphology change takes place on the external surface of the CCDC due to the surface modification of PANI, which indicates that PANI is coated on the external surface of the CCDC.

Nitrogen sorption isotherms were measured for calculating SSA, pore volumes and pore size distribution (PSD) in terms of the Bruauer–Emmet–Teller (BET) equation and Barrett–Joiner–Halenda (BJH) method. Fig. 4 shows the typical adsorption/desorption isotherms of N_2 at 77 K and their pore size distributions. The pore characteristics of the CCDC and CCDC/PANI composite are shown in Table 1. In Fig. 4(a), a hysteresis loop was observed, which indicated that the structure of the composite consisted of micropore and mesopore and the composite was beneficial to electrolyte ion movement. After CCDC coated by PANI, the BET specific surface area, pore volume and pore size decreased remarkably, which revealed that the surface and the wall of pores of CCDC were coated with PANI, and the same results can be confirmed by the morphologies shown in Fig. 3.

3.2. Electrochemical characterization

In order to evaluate the electrochemical characteristics of CCDC/PANI composite, cyclic voltammetry (CV) and galvanostatic charge/discharge were used to characterize the electrochemical capacitance performance. Fig. 5(a) shows cyclic voltammograms (within the potential window from −0.2 to 0.8 V vs. SCE) at different scan rates for the CCDC/PANI electrodes. It can be found that the capacitance characteristic of the PANI phase is different from that of the electric double layer capacitance (CCDC), which would produce a CV curve close to the ideal rectangular shape. Two redox peaks in Fig. 5 are attributed to the redox transition of PANI between a semiconducting state (leucoemeraldine form) and a conducting sate (polaronic emeraldine form) and the emeraldine–pernigraniline transformation [21]. With the increasing of scanning rate, the redox

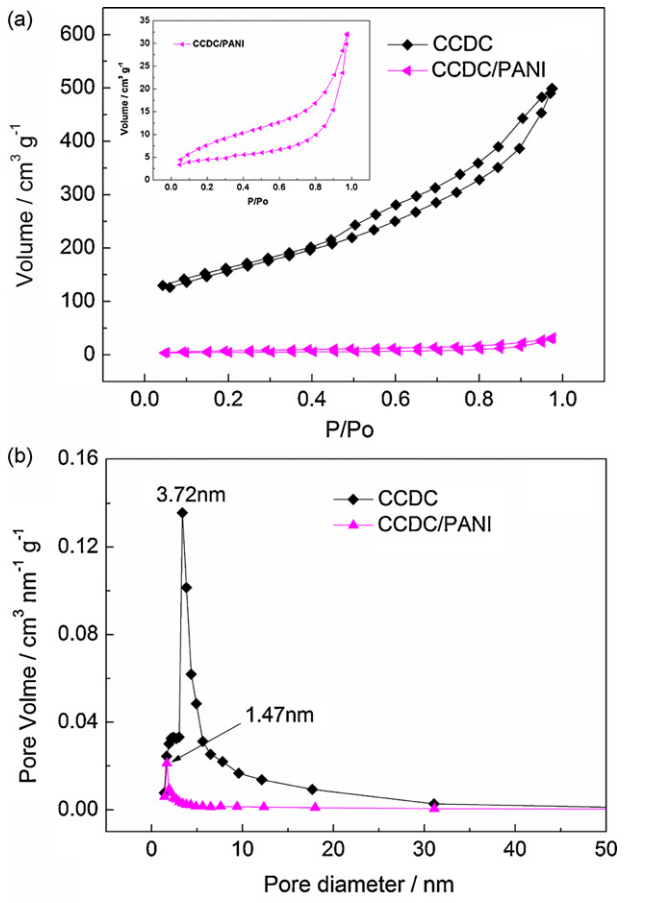

Fig. 4. Nitrogen adsorption isotherms at 77 K (a) and pore size distribution plots (b) of CCDC and CCDC/PANI composites.

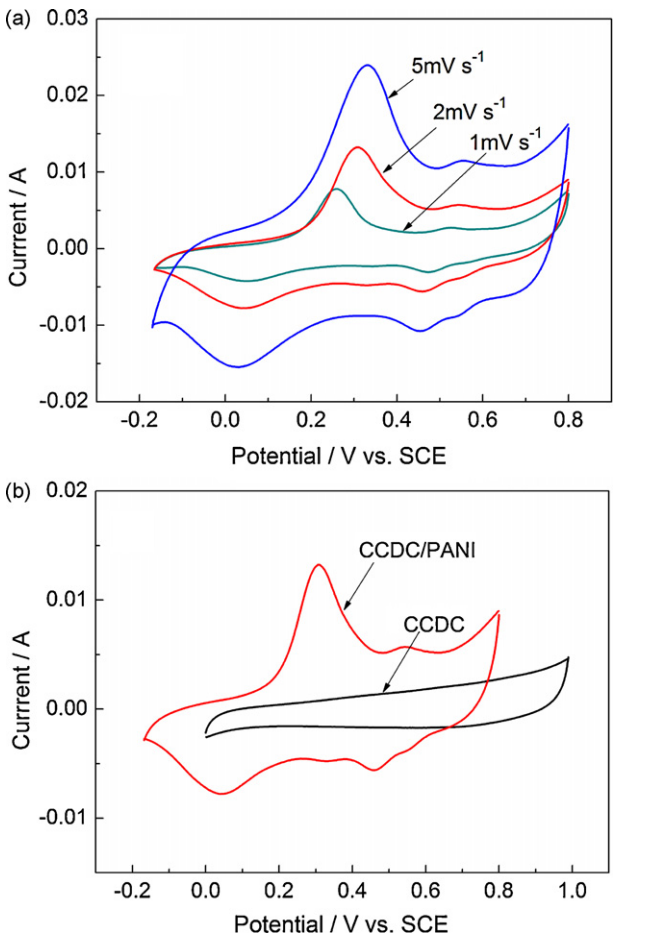

Fig. 5. Cyclic voltammograms for (a) CCDC/PANI electrodes at different scan rates and (b) the comparison of CCDC and CCDC/PANI composite at 2 mV s^{-1}.

current of CCDC/PANI electrode increases clearly, indicating its good rate ability. It is shown that higher capacitances are obtained from the CCDC/PANI composite at the applied scan rates. The maximum specific capacitance of CCDC/PANI electrode was 713.4 F g^{-1} at 1 mV s^{-1} from the CV curve according to Eq. (3) [22].

$$C \equiv \frac{Q}{V} = \int \frac{idt}{\Delta V} \tag{3}$$

where i is a sampled current, dt is a sampling time span, and ΔV is a total potential deviation of the voltage window.

Cyclic voltammograms for the CCDC electrode and CCDC/PANI composite electrodes at 2 mV s^{-1} are shown in Fig. 5(b). Comparing the CV of CCDC, it can be found that CCDC/PANI composite electrode has two distinct couples of redox peaks, and the area surrounded by CV curve is apparently larger than one of the CCDC electrode, indicating that the CCDC/PANI electrode has much more specific capacitance.

Table 2 tabulates the specific capacitances of CCDC and CCDC/PANI composite at different potential sweep rates, which were calculated according to Eq. (3) based on CV measurements. It can be found from Table 2 that the specific capacitances of CCDC/PANI electrodes are obviously higher than that of CCDC at every given scanning rate. The reason is probably that the capacitance of the CCDC/PANI electrodes is combination of double layer capacitance (CCDC) and Faradaic pseudocapacitance (PANI).

The charge/discharge curves of CCDC/PANI electrodes measured at different current densities within a potential window (−0.2 to 0.8 V vs. SCE) are showed in Fig. 6(a). As shown in Fig. 6(a), discharge time increased distinctly with current density decreasing, the specific capacitance of CCDC/PANI composite can be known from Eq. (4) [16,23].

$$C_m = \frac{C}{m} = \frac{I \times t}{\Delta V \times m} \tag{4}$$

where C_m is the specific capacitance (F g^{-1}), I is the charge/discharge current (A), t is the discharge time (s), ΔV is the range of the discharge (V), and m is the mass of the active material (g).

In Fig. 6(b), the comparison of galvanostatic charge/discharge curves for the CCDC electrode and CCDC/PANI composite electrode at 0.5 A g^{-1} was given. Comparing with the charge/discharge curve of CCDC, in which the potential varies nearly linearly with time, while curves of CCDC/PANI electrodes deviate from ideal linear

Table 1
The pore characteristics of CCDC and CCDC/PANI composite.

	BET-SSA (m^2 g^{-1})	Average aperture (nm)	Pore volume (cm^3 g^{-1})
CCDC	658	3.72	0.729
CCDC/PANI	14.8	1.67	0.426

Table 2
The specific capacitances of CCDC and CCDC/PANI composite.

	Specific capacitance of supercapacitors (F g^{-1})			
	1 mV s^{-1}	2 mV s^{-1}	5 mV s^{-1}	10 mV s^{-1}
CCDC	154.0	143.5	132.9	116.2
CCDC/PANI	713.4	661.2	601.4	531.6

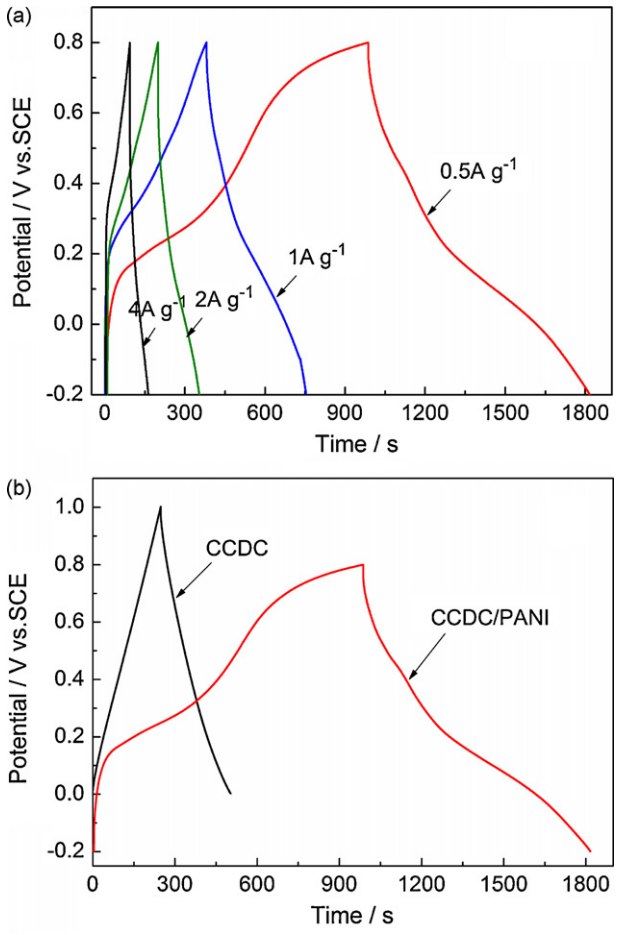

Fig. 6. Charge/discharge curves for (a) CCDC/PANI electrodes at different current densities and (b) comparison of CCDC and CCDC/PANI composite at 0.5 A g^{-1}.

line, indicating that the specific capacitance of the composite electrode is composed of both the double layer capacitance of CCDC and Faradaic capacitance of PANI.

In order to gain a further understanding on the electrochemical performance of CCDC/PANI composite materials, CCDC and CCDC/PANI were used as electrode active materials of symmetrical coin supercapacitor, respectively. The dependences of the specific capacitance of the two coin supercapacitor with charge/discharge cycle number are shown in Fig. 7. It is found that the CCDC and CCDC/PANI supercapacitors have demonstrated a very long cycle life under shallow depths of discharge. The specific capacitance of the coin supercapacitor can be known from Eq. (5) [24].

$$C = \frac{Q}{mV} = 3600 \times 0.001 \times \frac{C*}{mV} = 3.6 \times \frac{C*}{mV} \quad (5)$$

where C is the specific capacitance of the supercapacitor, F g^{-1}; Q is the electric quantity, C; C^* is the capacitance measured, mAh; m is the weight of simple electrode, g; V is the range of the charge/discharge, V.

The capacitance retention of the two coin supercapacitors is 98.7% and 80.1% over 1000 cycles, respectively. Besides, the specific capacitance of CCDC/PANI supercapacitor is markedly higher than that of CCDC supercapacitor, which indicates that the CCDC/PANI will be a promising electrode active material for long-term supercapacitors applications. The capacitance (Fig. 7) losses of CCDC/PANI composite electrodes are obviously larger than that of CCDC, indicating that larger PANI loading leads to worse cycle performance. Larger PANI loading results in larger scale of PANI phase, which tends to crack during charge–discharge process and then part of

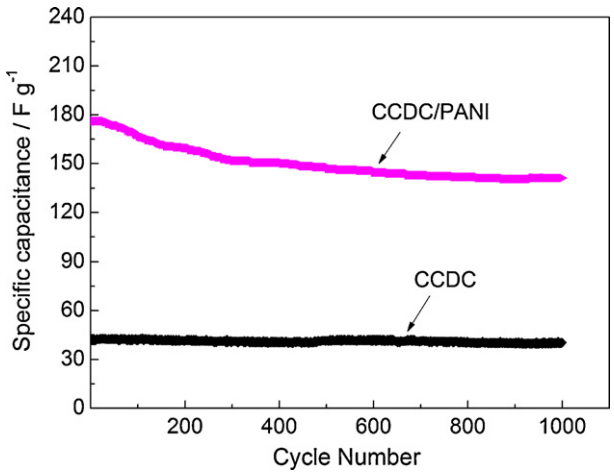

Fig. 7. Cycle life of CCDC and CCDC/PANI supercapacitors within the potential window −0.2 to 0.8 V vs. SCE.

the PANI deposits loses contact with the CCDC, resulting in not only poor transport of electrons but also poor cycle stability [25,26]. Therefore, future work should focus on the improvement of cyclic stability of the CCDC/PANI composite and thus increase its cyclic life.

Fig. 8 is the Ragone plot of the CCDC and CCDC/PANI supercapacitors. Energy density and power density are calculated using Eqs. (6) and (7) [27]

$$E = \frac{1}{2}C(\Delta V)^2 \quad (6)$$

$$P = \frac{I\Delta V}{2m} \quad (7)$$

where C is the capacitance of the capacitor, it is calculated according to Eq. (4); I, ΔV and m represent discharge current, range of the charge/discharge, the mass of active materials, respectively. It can be found that the CCDC and CCDC/PANI supercapacitors achieved an energy density of 24.25 and 67.5 Wh kg^{-1}, respectively. Besides, supercapacitors based on both the CCDC and CCDC/PANI composite have an excellent power performance. Moreover, with the increasing of the power density, the energy density of the CCDC/PANI composite supercapacitors decreased slightly faster than that of the CCDC supercapacitors because the speed of the redox reactions within the PANI is not as fast as the formation of the electric double layer in the CCDC electrode.

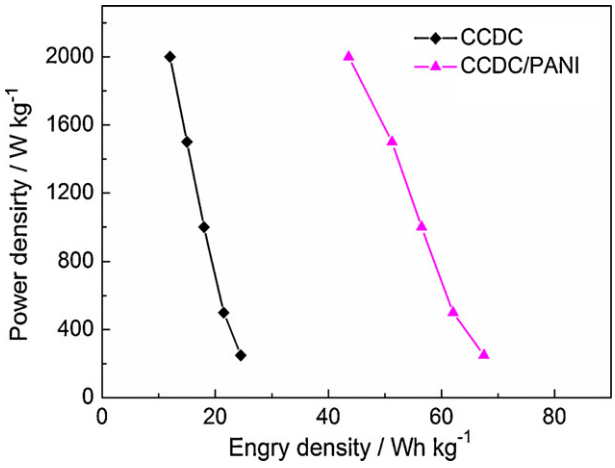

Fig. 8. Ragone plots of the CCDC and CCDC/PANI supercapacitors.

4. Conclusion

CCDC/PANI composite was synthesized by in situ chemical oxidation polymerization of aniline adsorbed on CCDC. The capacitance of the CCDC/PANI supercapacitor is markedly higher than one of CCDC supercapacitor since the capacitance of the CCDC/PANI is combination of double layer capacitance (CCDC) and Faradaic pseudocapacitance (PANI). CCDC/PANI composite in the application of supercapacitor showed excellent electrochemical performances, such as high specific capacitance, high energy density and stable cycle life. The specific capacitance of CCDC/PANI electrode calculated from CV curve is as high as 713.4 F g^{-1} at 1 mV s^{-1} compared with 154.0 F g^{-1} of CCDC electrode. Besides, the capacitance retention of the coin supercapacitor using CCDC/PANI composite as electrode active material was up to 80.1% after 1000 cycles. Therefore, it is obviously proved that the CCDC/PANI composite is a promising electrode material for the applications of supercapacitors.

Acknowledgements

This work was financially supported by the National Natural Science Foundation of China (Grant No. 20871101) and Key Project of Education Department of Hunan Province Government (Grant No. 08A067).

References

[1] M. Winter, R.J. Brodd, Chem. Rev. 104 (2004) 4245–4270.
[2] J.R. Miller, A.F. Burke, Electrochem. Soc. Interface 17 (2008) 44–48.
[3] S.R. Kwang, G.L. Young, M.K. Kang, et al., Synth. Met. 153 (2005) 89–92.
[4] B.Z. Fang, L. Binder, J. Phys. Chem. B 110 (2006) 7877–7882.
[5] P. Kuhn, A. Forget, D.S. Su, A. Thomas, M. Antonietti, J. Am. Chem. Soc. 130 (2008) 13333–13337.
[6] J. Li, X.Y. Wang, Y. Wang, Q.H. Huang, S. Gamboa, P.J. Sebastian, J. Non-Cryst. Solids 354 (2008) 19–24.
[7] K.X. Wang, Y.G. Wang, Y.R. Wang, E. Hosono, H.S. Zhou, J. Phys. Chem. C 113 (2009) 1093–1097.
[8] L.J. Ci, S.M. Manikoth, X.S. Li, R. Vajtai, P.M. Ajayan, Adv. Mater. 19 (2007) 3300–3303.
[9] Y. Gogotsi, S. Welz, D.A. Ersoy, M.J. McNallan, Nature 411 (2001) 283–287.
[10] J. Chmiola, G. Yushin, R. Dash, Y. Gogotsi, J. Power Sources 158 (2006) 765–772.
[11] C. Largeot, C. Portet, J. Chmiola, P.L. Taberna, Y. Gogotsi, P. Simon, J. Am. Chem. Soc. 130 (2008) 2730–2731.
[12] C.L. Dai, X.Y. Wang, Y. Wang, N. Li, J.L. Wei, Mater. Chem. Phys. 112 (2008) 461–465.
[13] C. Peng, S.W. Zhang, D. Jewell, G.Z. Chen, Prog. Nat. Sci. 18 (2008) 777–788.
[14] S.I. Cho, S.B. Lee, Acc. Chem. Res. 41 (2008) 699–707.
[15] Y.-R. Lin, H. Teng, Carbon 41 (2003) 2865–2871.
[16] L.X. Li, H.H. Song, Q.C. Zhang, J.Y. Yao, X.H. Chen, J. Power Sources 187 (2009) 268–274.
[17] Y.G. Wang, H.Q. Li, Y.Y. Xia, Adv. Mater. 18 (2006) 2619–2623.
[18] W.C. Chen, T.C. Wen, H. Teng, Electrochim. Acta 48 (2003) 641–649.
[19] H. F. An, Y. Wang, X. Y. Wang, N. Li, L. P. Zheng, J. Solid State Electrochem., doi:10.1007/s10008-009-0835-0, online Apr. 1, (2009).
[20] A. Subramania, S.L. Devi, Polym. Adv. Technol. 19 (2008) 725–727.
[21] C.C. Hu, J.Y. Lin, Electrochim. Acta 47 (2002) 4055–4067.
[22] J.H. Kima, Y.S. Lee, A.K. Sharma, C.G. Liu, Electrochim. Acta 52 (2006) 1727–1732.
[23] Q.H. Huang, X.Y. Wang, J. Li, C.L. Dai, S. Gamboa, P.J. Sebastian, J. Power Sources 164 (2007) 425–429.
[24] J. Li, X.Y. Wang, Q.H. Huang, S. Gamboa, P.J. Sebastian, J. Power Sources 160 (2006) 1501–1505.
[25] L.X. Li, H.H. Song, Q.C. Zhang, J.Y. Yao, X.H. Chen, J Power Sources 187 (2009) 268–274.
[26] H. Zhang, G.P. Cao, W.K. Wang, K. Yuan, B. Xu, W.F. Zhang, J. Cheng, Y.S. Yang, Electrochim. Acta 54 (2009) 1153–1159.
[27] Y. Xue, Y. Chen, M.L. Zhang, et al., Mater. Lett. 62 (2008) 3884–3886.